Chiral superconductivity in UTe_2 via emergent C_4 symmetry and spin-orbit coupling

Daniel Shaffer[1] and Dmitry V. Chichinadze[2]
[1]*Department of Physics, Emory University, 400 Dowman Drive, Atlanta, Georgia 30322, USA*
[2]*School of Physics and Astronomy, University of Minnesota, Minneapolis, Minnesota 55455, USA*

(Received 25 April 2022; revised 13 June 2022; accepted 24 June 2022; published 5 July 2022)

A lot of attention has been drawn to superconductivity in UTe_2, with suggestions of time-reversal symmetry-breaking triplet chiral superconducting order parameter. The chirality of the order parameter has been attributed to an accidental near degeneracy of two superconducting components belonging to one-dimensional (1D) irreducible representations (irreps) B_{2u} and B_{3u} of the relevant D_{2h} point group, and it has been argued that the chiral $B_{2u} + iB_{3u}$ combination is selected by ferromagnetic fluctuations. In this work we present a possible explanation of the near degeneracy as a result of an accidental C_4 symmetry of the band structure, with the superconducting order parameter belonging to the 2D E_u irrep of D_{4h} that uniquely descends to the sought-after $B_{2u} + iB_{3u}$ combination. We show that the C_4 symmetry is emergent at the level of the interactions using a renormalization group calculation and argue that the chiral combination of the order parameter is favored when spin-orbit coupling is added to the model.

DOI: 10.1103/PhysRevB.106.014502

I. INTRODUCTION

Recent experiments suggest that UTe_2 may be a chiral triplet superconductor (SC) [1–3] (see also Ref. [4] for a recent review). In particular, SC has been observed in extremely high magnetic fields for all field directions, including re-entrant SC [5] possibly due to the orbital effect [6–8], and there are strong indications of spontaneous time-reversal symmetry (TRS) breaking [1–3,9]. However, UTe_2 is strongly orthorombic with a D_{2h} point group symmetry which has only one-dimensional (1D) irreducible representations (irreps). This poses a problem since the realization of chiral superconductivity requires a gap function with multiple degenerate components (meaning each component has the same critical temperature in the linearized gap equation), which is only guaranteed to happen for higher dimensional irreps [10]. To circumvent this issue, it has been proposed that there is an accidental near degeneracy of two gap components belonging to two different 1D irreps of D_{2h} that effectively act as a single 2D irrep.

Though the precise symmetry of the order parameter has not been conclusively established in experiment and several alternative proposals exist [4,11,12], the B_{2u} and B_{3u} irreps have been argued to most closely match the symmetries of some of the experimentally observed responses [9,13–15]. Magnetic fluctuations have also been invoked to explain why the chiral $B_{2u} + iB_{3u}$ combination, corresponding to $p \pm ip$ pairing in terms of angular harmonics, is preferred over the TRS preserving the $B_{2u} + B_{3u}$ combination [9,14,16]. The mechanism is consistent with first-principles calculations that indicate that the uranium f orbital is localized, giving rise to ferromagnetic fluctuations [15,17]. The choice of two order parameters with different symmetries is also supported by recent observation of two jumps in heat-capacity measurements indicating two phase transitions [14]. This is consistent with the fact that the accidental degeneracy is not expected to be exact. However, no apparent underlying reason for why those two particular irreps are present and are nearly degenerate has been offered.

In this work we propose a simple possible source of the near degeneracy and illustrate it using a simple minimal band-structure model. The model is not intended to closely match the band structure obtained in experiments and numerical simulations. However, it captures what we argue is the main qualitative feature of UTe_2: The quasi-1D nature of the Fermi surfaces. This is motivated by DFT calculations [15,17], ARPES data [18], and de Haas-van Alphen (dHvA) oscillations [19], suggesting that the itinerant electrons are largely constrained to perpendicular 1D U and Te chains. Our model, therefore, consists of two arrays of perpendicular wires made of U and Te atoms correspondingly. It is mathematically similar to models that have been used in the context of proximitized twisted quantum wires [20], crossed sliding Luttinger liquids [21,22], two-legged ladder models [23–26], and the quasi-1D model for Sr_2RuO_4 [27].

In the absence of interactions, we first show that the model has an *accidental* approximate D_{4h} symmetry of the Bogolyubov-de Gennes Hamiltonian which *does* have a 2D irrep E_u. Under the breaking of the accidental C_4 symmetry $D_{4h} \to D_{2h}$ and the two components of the E_u irrep descend to B_{2u} and B_{3u} irreps, in agreement with observations. Adding the interactions that include spin fluctuations, we find that under the renormalization group (RG) flow the intrachain coupling constants flow to the same values at least for some range of the bare coupling constant, even if the bare constants break the accidental C_4 symmetry. The result is an *emergent* D_{4h} symmetry. A related phenomenon has been conjectured for the two-channel Kondo lattice [28–31], though it was

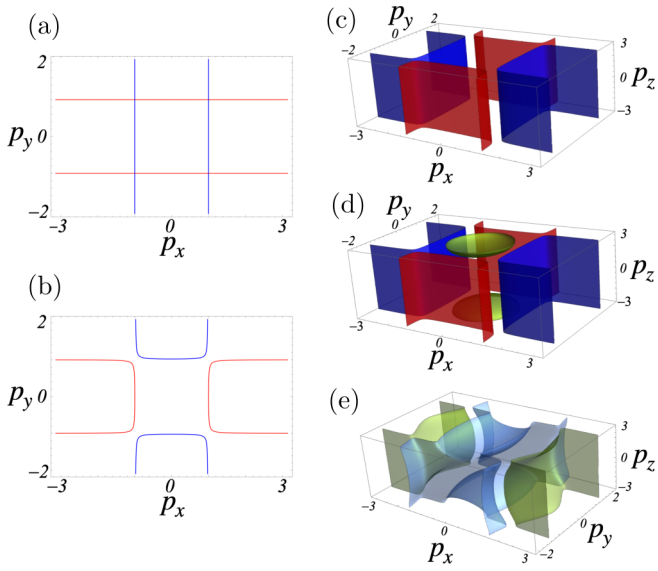

FIG. 1. Fermi surfaces of UTe_2 in various approximations. (a) Model without SOC assuming pure 1D dispersion along U (blue curves) and Te (red curves). We also show the ordering vectors corresponding to peaks in intra-atomic U (red arrows), intra-atomic Te (blue arrows), and interatomic (purple arrows) susceptibilities. (b), (c) Quasi-1D model with SOC shown in 2D and 3D BZs. (d) Quasi-1D model with an additional Z electron pocket without SOC between d and f U electrons. (e) Same as (d) but including SOC between d and f U electrons. Note that the Z electron pocket hybridizes with the X electron pocket as a result, forming a doughnut shape (actually a double doughnut once the walls of the BZ are identified). Cf. with DFT calculations and ARPES and dHvA data [13,15,18,19].

not supported by RG calculations [32]. The RG flow for our model also leads to a triplet instability belonging to the desired E_u irrep. Finally, we show that the free energy is minimized by a chiral $p + ip$ paired state when spin-orbit coupling (SOC) is included. Our approach thus provides a microscopic explanation of the observed TRS breaking triplet pairing and two superconducting transitions associated with chiral structure of the order parameter.

The structure of the paper is as follows. In Sec. II we introduce the free-fermion model and discuss the structure of Fermi surfaces. In Sec. III we discuss the approximate symmetry of BdG Hamiltonian and its effect on SC order parameters. Section IV is dedicated to the RG analysis of interactions and the emergence of effective C_4 symmetry. We show that the ground state is a chiral SC using the Landau functional for SC order parameters in Sec. V. We discuss our results and conclude in Sec. VI.

II. MINIMAL MODEL AND FERMI SURFACES

The actual Fermi surfaces of UTe_2 have been partially measured in ARPES experiments [18], but there are still a few issues that have not been resolved, in particular whether or not a pocket is present at the Z point in Brillouin zone (BZ). Nevertheless, the known features of the Fermi surfaces can be understood in a sequence of approximations (see Fig. 1). The relevant degrees of freedom originate from the p orbital holes of Te atoms and one electron each from the d and f orbitals of the U atoms. The U atoms form double chains while Te atoms form single chains running in the orthogonal direction. The role of the f electrons is the main unresolved question in the literature: in DFT calculations with intermediate interactions, they form the Z pockets, but at larger U the pockets are gapped out, possibly due to the Kondo physics [15,17]. We will mostly ignore the f electrons for simplicity, though they likely play an important indirect role in producing ferromagnetic spin fluctuations that we do include later in our interaction model below.

Neglecting the f electrons, the U double chains can be thought of as a single chain, and since the separation between the chains is much larger than the separation between atoms within the chain, to zeroth order the dispersions are 1D and can be described by a 2×2 $\mathbf{k} \cdot \mathbf{p}$ Hamiltonian (not including spin),

$$\mathcal{H}_0 = \begin{pmatrix} \frac{p_x^2}{2m_U} - \mu_U & 0 \\ 0 & -\frac{p_y^2}{2m_{Te}} - \mu_{Te} \end{pmatrix}. \tag{2.1}$$

In the simplest case, which we will adopt, $m_U = m_{Te}$ and $\mu_U = -\mu_{Te} = \mu$. This is, of course, somewhat far away from the real system but matches the qualitative features of the ARPES Fermi surface data surprisingly well. The Fermi surfaces in this approximation are simply straight lines, orthogonal for the electrons and holes [see Fig. 1(a)].

A. Corrections to the minimal model from SOC and the Z pocket

There are several properties of UTe_2 that the minimal model does not capture that we discuss here for completeness. First, an $\mathbf{L} \cdot \mathbf{S}$-type SOC is present in the real system. The SOC hybridizes the p and d orbitals, splitting the Fermi surfaces into an electron and a hole pocket centered at the Y and X points. For moderate values of SOC, the splitting is small and the pockets are nearly rectangular, as shown in Figs. 1(b) and 1(c). There are several symmetry-allowed SOC terms, but to capture the qualitative effect it is enough to include one,

$$\mathcal{H}_1 = \mathcal{H}_0 + \alpha \sigma^0 \tau^x = \begin{pmatrix} \frac{p_x^2}{2m} - \mu & \alpha \\ \alpha & -\frac{p_y^2}{2m} + \mu \end{pmatrix}, \tag{2.2}$$

where σ is the spin Pauli matrix, τ is the Pauli matrix in the space of U/Te degrees of freedom, and α is the SOC strength. Note we can take the SOC term to be nominally spin independent due to inversion symmetry.

As mentioned above, we also neglect the f-electron pocket at the Z point in BZ in our model, but in principle it can be included, as shown in Fig. 1(d). If present, it is in general hybridized with the Y pocket due to SOC between the d and the f uranium orbitals, resulting in a doughnut-shaped Fermi surface [see Fig. 1(e)]. We assume that even if the Z pocket is present, it participates only weakly in the superconducting condensate and so can be neglected. In contrast, though we can initially neglect the SOC between p and d orbitals, we will show in Sec. V that it has an important role in determining the

relative phase between the two components of the superconducting order parameter.

III. ACCIDENTAL APPROXIMATE SYMMETRY OF THE BOGOLYUBOV-DE GENNES HAMILTONIAN

We include superconductivity by considering the Bogolyubov-de Gennes (BdG) Hamiltonian in the absence of SOC,

$$\mathcal{H}_{Bdg} = \begin{pmatrix} \mathcal{H}_0(\mathbf{p}) & \hat{\Delta}(\mathbf{p}) \\ \hat{\Delta}^\dagger(\mathbf{p}) & -\mathcal{H}_0^*(-\mathbf{p}) \end{pmatrix} = \begin{pmatrix} \frac{p_x^2}{2m} - \mu & 0 & \Delta_U & 0 \\ 0 & -\frac{p_y^2}{2m} + \mu & 0 & \Delta_{Te} \\ \Delta_U^\dagger & 0 & -\frac{p_x^2}{2m} + \mu & 0 \\ 0 & \Delta_{Te}^\dagger & 0 & \frac{p_y^2}{2m} - \mu \end{pmatrix}, \tag{3.1}$$

where Δ_U and Δ_{Te} are 2×2 matrices in spin space. Note that due to inversion symmetry, the pairing is predominantly between two uranium electrons or two tellurium holes (i.e., between opposite sides of the Fermi surfaces), and the pairing between U and Te can be neglected as a result. In the BdG formalism we introduce the Nambu spinors $\Psi_{\tau\sigma}(\mathbf{p}) = (\psi_{\tau\sigma}(\mathbf{p}), \psi^\dagger_{\tau\sigma}(-\mathbf{p}))$ (τ labels U or Te), resulting in a twofold redundancy. This is accounted for by the antiunitary particle-hole symmetry (PHS) which acts as $\mathcal{C} = \varsigma^x \mathcal{K}$ where ς^x is a Pauli matrix acting on the new particle/hole degrees of freedom and $\mathcal{K}$ is complex conjugation. PHS in particular requires $\hat{\Delta}(\mathbf{p}) = -\hat{\Delta}^\dagger(-\mathbf{p})$.

We make the following observation: In the normal state with $\hat{\Delta} = 0$, the BdG Hamiltonian has a new unitary symmetry that is not present in the original Hamiltonian. The new symmetry is $C_4 \tau^x \varsigma^x$, where C_4 is a fourfold rotation symmetry taking $p_x \to p_y$ and $p_y \to -p_x$. This is intuitively clear: In the BdG Hamiltonian we introduce additional redundant copies of the Fermi surfaces but of opposite characters (electron instead of hole and vice versa). The full symmetry of the BdG Hamiltonian in the simplest version of our model is, therefore, not $D_{2h} \times \mathcal{P}$ ($\mathcal{P}$ being the PHS symmetry group) but rather $D_{4h} \times \mathcal{P}$. Of course the symmetry is only exact in our oversimplified model, but it remains an approximate symmetry as long as the neglected terms are not too large (we address some possible sources of such terms in Appendix A).

Since the effective point group is D_{4h}, the gap functions have to be classified according to irreps of D_{4h}, not D_{2h}. We note that D_{4h} has two 2D irreps, E_g and E_u, corresponding to singlet and triplet pairing, respectively. Since the symmetry is only approximate, the irreps of D_{4h} descend into irreps of D_{2h}. For E_u, the two components $E_u^{(1)}$ and $E_u^{(2)}$ descend into two different 1D irreps of D_{2h}, $E_u^{(1)} \to B_{2u}$ and $E_u^{(2)} \to B_{3u}$ [33]. Therefore the chiral E_u phase, if established, descends uniquely into the $B_{2u} + iB_{3u}$ phase, explaining the experimental observations and ruling out other proposed combinations (e.g., the nonunitary pairing proposed in Refs. [11,12]). Moreover, since the C_4 symmetry is broken, we expect the degeneracy between B_{2u} and B_{3u} also to be inexact, resulting in one of those two channels having higher T_c, in agreement with the two jumps seen in the specific-heat data [14].

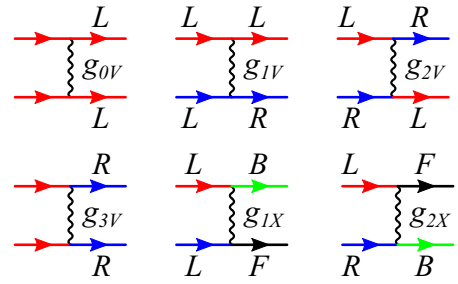

FIG. 2. Coupling constants g_{nA} with $g = u, J^{(j)}$; $n = 0, 1, 2, 3$; $A = V, X$ (the diagrams for $A = H$ are similar with $L \to B$ and $R \to F$).

A valid objection to the argument above is that it only holds for the noninteracting part of the Hamiltonian. The interactions, on the other hand, only have to respect the D_{2h} symmetry and not necessarily the accidental D_{4h}. As we show in the following section, however, the accidental C_4 symmetry of the noninteracting Hamiltonian leads to an *emergent* C_4 symmetry on the level of the interaction Hamiltonian within the RG approach.

IV. EMERGENT C_4 SYMMETRY OF THE INTERACTIONS UNDER RG FLOW

In this section we address the issue of the absence of C_4 symmetry at the interaction level by showing that the C_4 symmetry can be emergent within the RG paradigm. The key to the result is the quasi-1D nature of the system. Assuming that the interactions are dominant between sites within the chains and negligible between neighboring chains as well as between perpendicular chains, the interactions within the chains are essentially 1D and we can write down two sets of decoupled RG equations for each set of parallel chains. We label those chains H and V for horizontal (U) and vertical (Te). Note that in 1D one can solve the interaction problem exactly by bosonization, which has also been done for crossed wire networks to obtain the so-called crossed sliding Luttinger liquid [21,22]. Before introducing the coupling between the H and V wires, we assume that they are in the Luttinger liquid regime, i.e., all the RG flows are at most marginal (or else irrelevant). The bare coupling constants of H and V wires are otherwise not assumed to be related and so explicitly break the C_4 symmetry. We then include interchain coupling between H and V wires as a perturbation and find that it results in an instability (i.e., a relevant flow in RG). The general argument is that since the instability is driven by the infinitesimal interchain interactions, the final fixed trajectory of the RG flow does not sensitively depend on the particular choice of the intrachain coupling constants (at least for some range) and is therefore C_4 symmetric. We verify numerically that the H and V coupling constants are equal for some choices of the bare interactions, i.e., there is an emergent C_4 symmetry.

In 1D, the Fermi surfaces are two points, and as usual we label them L and R (left and right) for the horizontal chains and B and F (bottom and front) for the vertical chains. The interactions within the vertical chains then have the following

form (see Fig. 2),

$$\begin{aligned} H_V =& \frac{1}{2}\sum u_{0V} c^\dagger_{A\alpha}\delta_{\alpha\alpha'} c_{A\alpha'} c^\dagger_{A\beta}\delta_{\beta\beta'} c_{A\beta'} \\ &+ \frac{1}{2}\sum u_{1V} c^\dagger_{B\alpha}\delta_{\alpha\alpha'} c_{B\alpha'} c^\dagger_{F\beta}\delta_{\beta\beta'} c_{F\beta'} \\ &+ \frac{1}{2}\sum u_{2V} c^\dagger_{B\alpha}\delta_{\alpha\alpha'} c_{F\alpha'} c^\dagger_{F\beta}\delta_{\beta\beta'} c_{B\beta'} \\ &+ \frac{1}{2}\sum u_{3V} c^\dagger_{B\alpha}\delta_{\alpha\alpha'} c_{F\alpha'} c^\dagger_{B\beta}\delta_{\beta\beta'} c_{F\beta'} \\ &+ \frac{1}{2}\sum J^{(j)}_{0V} c^\dagger_{A\alpha}\sigma^j_{\alpha\alpha'} c_{A\alpha'} c^\dagger_{A\beta}\sigma^j_{\beta\beta'} c_{A\beta'} \\ &+ \frac{1}{2}\sum J^{(j)}_{1V} c^\dagger_{B\alpha}\sigma^j_{\alpha\alpha'} c_{B\alpha'} c^\dagger_{F\beta}\sigma^j_{\beta\beta'} c_{F\beta'} \\ &+ \frac{1}{2}\sum J^{(j)}_{2V} c^\dagger_{B\alpha}\sigma^j_{\alpha\alpha'} c_{F\alpha'} c^\dagger_{F\beta}\sigma^j_{\beta\beta'} c_{B\beta'} \\ &+ \frac{1}{2}\sum J^{(j)}_{3V} c^\dagger_{B\alpha}\sigma^j_{\alpha\alpha'} c_{F\alpha'} c^\dagger_{B\beta}\sigma^j_{\beta\beta'} c_{F\beta'} + \text{H.c.} \end{aligned} \tag{4.1}$$

(A is summed over B and F while j is summed over x, y, z). Within the horizontal chains we have similarly (with A summed over L and R instead),

$$\begin{aligned} H_H =& \frac{1}{2}\sum u_{0H} d^\dagger_{A\alpha}\delta_{\alpha\alpha'} d_{A\alpha'} d^\dagger_{A\beta}\delta_{\beta\beta'} d_{A\beta'} \\ &+ \frac{1}{2}\sum u_{1H} d^\dagger_{L\alpha}\delta_{\alpha\alpha'} d_{L\alpha'} d^\dagger_{R\beta}\delta_{\beta\beta'} d_{R\beta'} \\ &+ \frac{1}{2}\sum u_{2H} d^\dagger_{L\alpha}\delta_{\alpha\alpha'} d_{R\alpha'} d^\dagger_{R\beta}\delta_{\beta\beta'} d_{L\beta'} \\ &+ \frac{1}{2}\sum u_{3H} d^\dagger_{L\alpha}\delta_{\alpha\alpha'} d_{R\alpha'} d^\dagger_{L\beta}\delta_{\beta\beta'} d_{R\beta'} \\ &+ \frac{1}{2}\sum J^{(j)}_{0H} d^\dagger_{A\alpha}\sigma^j_{\alpha\alpha'} d_{A\alpha'} d^\dagger_{A\beta}\sigma^j_{\beta\beta'} d_{A\beta'} \\ &+ \frac{1}{2}\sum J^{(j)}_{1H} d^\dagger_{L\alpha}\sigma^j_{\alpha\alpha'} d_{L\alpha'} d^\dagger_{R\beta}\sigma^j_{\beta\beta'} d_{R\beta'} \\ &+ \frac{1}{2}\sum J^{(j)}_{2H} d^\dagger_{L\alpha}\sigma^j_{\alpha\alpha'} d_{R\alpha'} d^\dagger_{R\beta}\sigma^j_{\beta\beta'} d_{L\beta'} \\ &+ \frac{1}{2}\sum J^{(j)}_{3H} d^\dagger_{L\alpha}\sigma^j_{\alpha\alpha'} d_{R\alpha'} d^\dagger_{L\beta}\sigma^j_{\beta\beta'} d_{R\beta'} + \text{H.c.} \end{aligned} \tag{4.2}$$

Finally, the perturbing interactions between the two chains are

$$\begin{aligned} H_X =& \frac{1}{2}\sum u_{1X} d^\dagger_{L\alpha}\delta_{\alpha\alpha'} c_{B\alpha'} d^\dagger_{R\beta}\delta_{\beta\beta'} c_{F\beta'} \\ &+ \frac{1}{2}\sum u_{2X} d^\dagger_{L\alpha}\delta_{\alpha\alpha'} c_{F\alpha'} d^\dagger_{R\beta}\delta_{\beta\beta'} c_{B\beta'} \\ &+ \frac{1}{2}\sum J^{(j)}_{1X} d^\dagger_{L\alpha}\sigma^j_{\alpha\alpha'} c_{B\alpha'} d^\dagger_{R\beta}\sigma^j_{\beta\beta'} c_{F\beta'} \\ &+ \frac{1}{2}\sum J^{(j)}_{2X} d^\dagger_{L\alpha}\sigma^j_{\alpha\alpha'} c_{F\alpha'} d^\dagger_{R\beta}\sigma^j_{\beta\beta'} c_{B\beta'} + \text{H.c.} \end{aligned} \tag{4.3}$$

These are the only momentum-conservation allowed interactions that are relevant for the RG flows; u's correspond to density-density interactions, while J's correspond to spin fluctuations; we use g as a generic label for coupling constants of either type. We include spin fluctuations as they have been suggested to mediate the triplet superconductivity [9,14,34–37]; g_0 are intrapocket interactions that as we will see do not flow under the RG and do not affect other flows and so henceforth can be ignored; g_1 are interpocket interactions, g_2 are exchange interactions, and g_3 are umklapp processes only allowed at half filling (we will later drop the g_3 terms and assume we are not at half filling). Note that g_{nH} and g_{nV} coupling constants have to be real by TRS and/or by mirror/rotation symmetries. The interchain interactions g_{nX} may, on the other hand, be complex due to the absence of C_4 symmetry, but note that due to the xz and yz mirror symmetries that exchange B/F and L/R labels, respectively, while keeping the other two fixed, we must have $g_{1X} = g_{2X}$, and we will therefore label them simply as u_X and $J^{(j)}_X$ below.

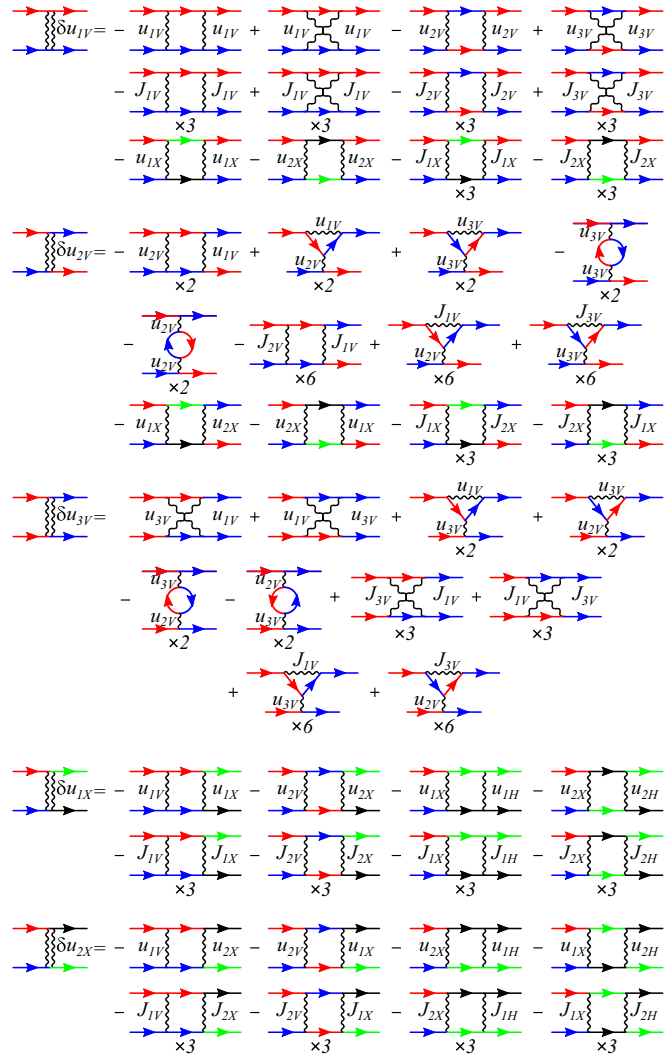

FIG. 3. Diagrammatic representation of RG equations for density-density interactions u_i. Note the corrections coming from the spin J couplings that generate u_{nA} even if they are absent initially; see Appendix B.

For simplicity, we will assume that the spin fluctuations are isotropic, $J^{(x)}_{nA} = J^{(y)}_{nA} = J^{(z)}_{nA} = J_{nA}$ ($n = 0, 1, 2, 3$, $A = H, V$). In that case we obtain the following RG equations (see Figs. 3

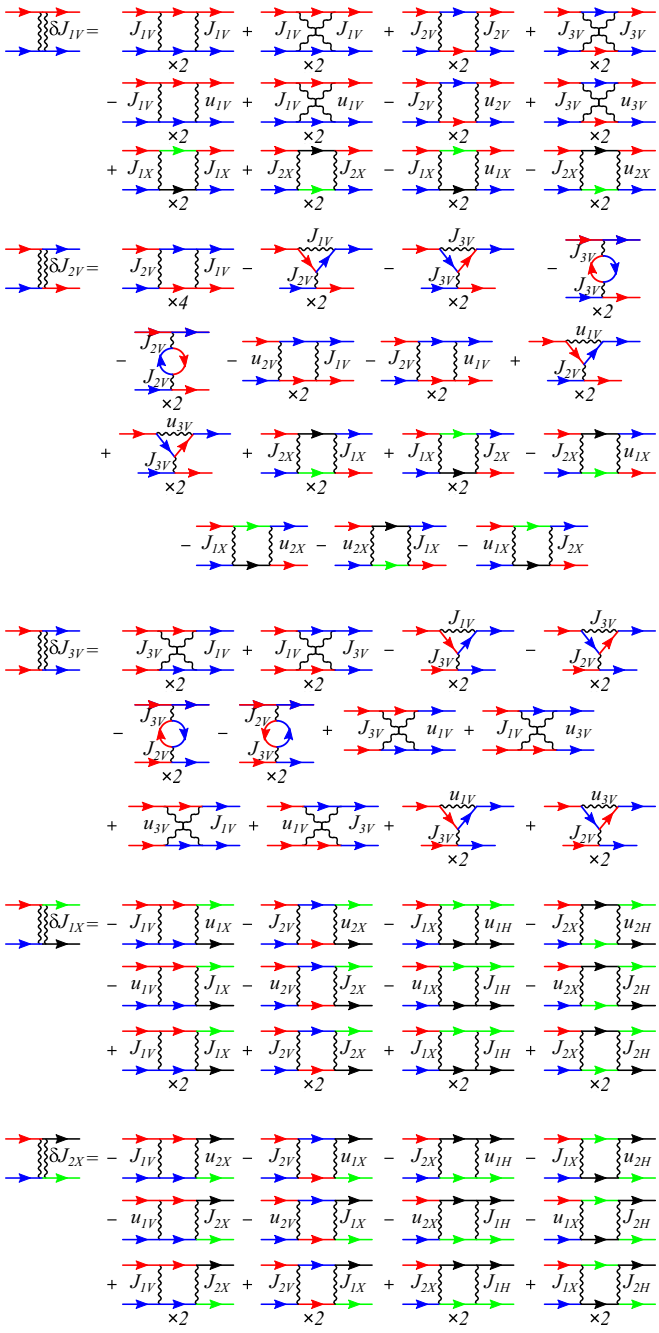

FIG. 4. Diagrammatic representation of RG equations for spin-spin interactions J_{nA}. Note the corrections coming from the terms involving density-density u_{nA}.

and 4),

$$\dot{u}_{1V} = -u_{2V}^2 + u_{3V}^2 - 3J_{2V}^2 + 3J_{3V}^2 - 2|u_X|^2 - 6|J_X|^2 \quad (4.4)$$

$$\dot{u}_{2V} = -2u_{2V}^2 - 6J_{1V}J_{2V} + 6u_{3V}J_{3V} + 6u_{2V}J_{1V} - 2|u_X|^2 - 6|J_X|^2 \quad (4.5)$$

$$\dot{u}_{3V} = 4u_{1V}u_{3V} - 2u_{2V}u_{3V} + 6u_{3V}J_{1V} + 6u_{2V}J_{3V} + 6J_{1V}J_{3V} \quad (4.6)$$

$$\dot{J}_{1V} = 2\big(-u_{2V}J_{2V} + u_{3V}J_{3V} + 2J_{1V}^2 + J_{2V}^2 + J_{3V}^2\big) - 4\mathrm{Re}[u_X^* J_X] + 4|J_X|^2 \quad (4.7)$$

$$\dot{J}_{2V} = 2\big(u_{3V}J_{3V} - u_{2V}J_{1V} - J_{2V}^2 + J_{1V}J_{2V} - 2J_{3V}^2\big) - 4\mathrm{Re}[u_X^* J_X] + 4|J_X|^2 \quad (4.8)$$

$$\dot{J}_{3V} = 2(2u_{1V}J_{3V} + u_{3V}J_{1V} + u_{3V}J_{2V}) + 2(J_{1V}J_{3V} - 3J_{2V}J_{3V}) \quad (4.9)$$

$$\dot{u}_X = -(u_{1V} + u_{2V})u_X - u_X^*(u_{1H} + u_{2H}) - 3(J_{1V} + J_{2V})J_X - 3J_X^*(J_{1H} + J_{2H}) \quad (4.10)$$

$$\dot{J}_X = -(u_{1V} + u_{2V})J_X - u_X(J_{1V} + J_{2V}) - u_X^*(J_{1H} + J_{2H}) - (u_{1H} + u_{2H})J_X^* + 2(J_{1V} + J_{2V})J_X + 2J_X^*(J_{1H} + J_{2H}), \quad (4.11)$$

with a similar set of equations for g_{nH}; the dot indicates a derivative with respect to the RG time $t = \log \frac{\Lambda}{E}$ where Λ is the high-energy cutoff and E is the energy scale above which the high-energy modes have been integrated out in the RG flow. The details of the RG, including equations for nonisotropic spin fluctuations, can be found in Appendix B. Here we assumed for simplicity that the DOS's of H and V chains are equal. If the DOS's are different we can recover the same equations by rescaling the coupling constants as $\tilde{g}_V = \nu_V g_V$, $\tilde{g}_H = \nu_H g_H$ and $\tilde{g}_X = \sqrt{\nu_V \nu_H} g_X$, so that the form of the equations is the same. For simplicity, we will keep assuming that the DOS's are equal, i.e., the noninteracting part of the Hamiltonian is C_4 symmetric. We also henceforth set the umklapp processes g_{3A} to zero, as those generally lead to instabilities in 1D and we are interested in the Luttinger regime in the absence of interchain interactions g_X. As mentioned above, this is justified on physical grounds as we do not expect both sets of chains to be exactly at half filling.

The resulting RG flow is shown in Fig. 5 (see caption and below for bare coupling constant values). As claimed, with the chosen values of the bare coupling constants the quantities $(g_{nV} - g_{nH})/(g_{nV} + g_{nH})$ flow to zero while $g_{nV} + g_{nH}$ diverges, implying that $g_{nV} = g_{nH}$ at the fixed point at infinity, i.e., there is an emergent C_4 symmetry. This is true for a relatively wide range of the bare coupling constants, assuming no instabilities in the absence of interchain interactions g_X (there are also other fixed trajectories we observed along which $g_{nV} = 0$ or $g_{nH} = 0$). This result matches the conjectured RG flow proposed for the related two-channel Kondo lattice [28]—the two initially different couplings become equal under the RG flow.

A. Vertex flow equations

Though we find an emergent C_4 symmetry of the interactions, we also need to show that triplet superconductivity belonging to the E_u irrep is the leading instability. To show that, we introduce test vertices

$$\Delta_{LR}^{(\mu)}(\sigma^\mu i\sigma^y)_{\alpha\beta} d_{\mathbf{p},L,\alpha}^\dagger d_{\mathbf{p},R,\beta}^\dagger + \mathrm{H.c.}$$
$$\Delta_{BF}^{(\mu)}(\sigma^\mu i\sigma^y)_{\alpha\beta} c_{\mathbf{p},B,\alpha}^\dagger c_{\mathbf{p},F,\beta}^\dagger + \mathrm{H.c.}$$
$$\Delta_{RL}^{(\mu)}(\sigma^\mu i\sigma^y)_{\alpha\beta} d_{\mathbf{p},R,\alpha}^\dagger d_{\mathbf{p},L,\beta}^\dagger + \mathrm{H.c.}$$
$$\Delta_{FB}^{(\mu)}(\sigma^\mu i\sigma^y)_{\alpha\beta} c_{\mathbf{p},F,\alpha}^\dagger c_{\mathbf{p},B,\beta}^\dagger + \mathrm{H.c.} \quad (4.12)$$

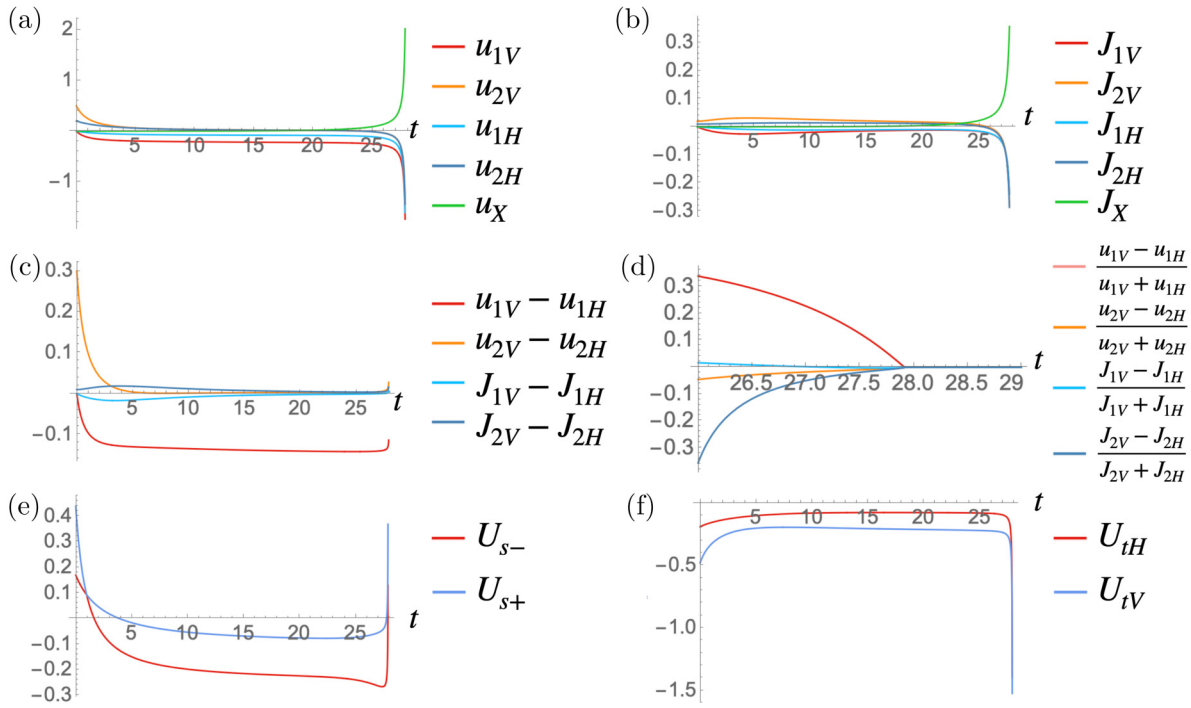

FIG. 5. RG flow as a function of the RG time $t = \log \frac{\Lambda}{E}$ for the following values of the bare coupling constants: $u_{2H} = 0.2$, $J_{2H} = 0.01$, $u_{2V} = 0.5$, $J_{2V} = 0.02$, $u_X = 0.001$, and $J_X = 0.0003$. Panels (a) and (b) show the flow of the density-density and spin-fluctuation mediated interactions, respectively; the intrachain coupling constants all flow to negative values while the interchain couplings u_X and J_X flow to positive values. Panel (c) shows the flow of the differences of intrachain coupling between V and H chains, (d) shows the same differences normalized by the sums. Note that the latter flow to zero at the instability, indicating an emergent C_4 symmetry. Panels (e) and (f) show the effective interactions $U_{s\pm}$ in the singlet and U_{tV} and U_{tH} in the triplet pairing channels, respectively [see Eqs. (4.15–4.16)], with negative/positive values corresponding to attraction/repulsion. We thus find that the triplet channel wins under the RG flow with the given bare coupling constants. Note that while U_{tV} and U_{tH} are unequal at the beginning of the flow, their difference vanishes asymptotically at the critical RG scale as follows from Eq. (4.15).

and study their RG flow, including the competition between the singlet and the triplet channels. The relevant diagrams are shown in Fig. 6. Note that due to anticommutation relations, we have the PHS relations

$$\begin{aligned}
\Delta^{(0)}_{LR} &= \Delta^{(0)}_{RL} = \Delta^{(0)}_{H} \\
\Delta^{(0)}_{BF} &= \Delta^{(0)}_{FB} = \Delta^{(0)}_{V} \\
\Delta^{(j)}_{LR} &= -\Delta^{(j)}_{RL} = \Delta^{(j)}_{H} \\
\Delta^{(j)}_{BF} &= -\Delta^{(j)}_{FB} = \Delta^{(0)}_{V},
\end{aligned} \tag{4.13}$$

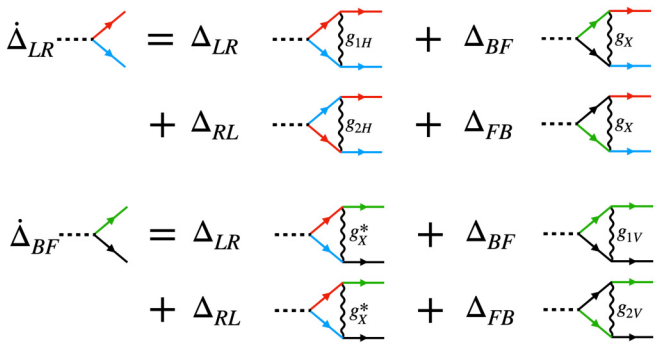

FIG. 6. Diagrammatic representation of the SC vertex flow equations. The spin sum evaluation is presented in Appendix B.

where $j = x, y, z$ correspond to the triplet components and $\mu = 0$ is the singlet component of the gap functions. The RG flow equations of the vertices $\Delta^{(\mu)}_H$ and $\Delta^{(\mu)}_V$ are as follows [38]:

$$\begin{aligned}
\dot{\Delta}^{(0)}_H &= -(u_{1H} + u_{2H} - 3J_{1H} - 3J_{2H})\Delta^{(0)}_H \\
&\quad - 2(u_X - 3J_X)\Delta^{(0)}_V \\
\dot{\Delta}^{(0)}_V &= -(u_{1V} + u_{2V} - 3J_{1V} - 3J_{2V})\Delta^{(0)}_V \\
&\quad - 2(u^*_X - 3J^*_X)\Delta^{(0)}_H \\
\dot{\Delta}^{(j)}_H &= -(u_{1H} - u_{2H} + J_{1H} - J_{2H})\Delta^{(j)}_H \\
\dot{\Delta}^{(j)}_V &= -(u_{1V} - u_{2V} + J_{1V} - J_{2V})\Delta^{(j)}_V.
\end{aligned} \tag{4.14}$$

The relevant spin sums are shown in Appendix B. Importantly, the H and V triplet components are decoupled (thanks to the cancellation due to the mirror symmetries of the D_{2h} point group). As a result, if the C_4 symmetry emerges at the RG fixed point, the triplet H and V channels become degenerate, meaning that they belong to a 2D irrep.

The effective pairing triplet interactions are simply

$$U_{tA} = u_{1A} - u_{2A} + J_{1A} - J_{2A}, \tag{4.15}$$

with $A = H, V$. The effective singlet interactions are found by diagonalizing the matrix equation for the flow of $\Delta^{(0)}_H$ and

$\Delta_V^{(0)}$, with

$$U_{s\pm} = \tfrac{1}{2}\big(U_{sVH} \pm \sqrt{U_{sVH}^2 + 16|u_X - 3J_X|^2}\big), \tag{4.16}$$

where

$$\begin{aligned} U_{sVH} =& u_{1H} + u_{1V} + u_{2H} + u_{2V} - 3J_{1H} \\ & - 3J_{1V} - 3J_{2H} - 3J_{2V}. \end{aligned} \tag{4.17}$$

Based on the flow equations, we then see that the triplet pairing is favored over the singlet pairing either for large negative exchange u_{2A} interactions or for large negative (i.e., ferromagnetic) spin fluctuations J_{1A}. However, the former is ruled out by our requirement that the interactions are marginal in the absence of interchain interactions g_X, while in the latter we find not to give rise to an emergent C_4 symmetry. Instead, we find that the desired solution is obtained for a larger positive u_{2A} and a smaller but sizable positive (i.e., anti-ferromagnetic) J_{2A}, with an even smaller u_X and an even smaller J_X.

As a concrete case we take the bare coupling constants to be $u_{2H} = 0.2$, $J_{2H} = 0.01$, $u_{2V} = 0.5$, $J_{2V} = 0.02$, $u_X = 0.001$, and $J_X = 0.0003$ and the rest zero. With these bare coupling constants the leading SC channel is indeed triplet and, moreover, U_{tV} and U_{tH} become equal as they diverge at the critical RG scale as can be verified from Eq. (4.15) and Fig. 6 (more precisely their difference vanishes asymptotically). This implies that the leading triplet SC channel belongs to a 2D E_u irrep of D_{4h}, as desired. Although the initial intrachain spin fluctuations are positive, i.e., antiferromagnetic, observe that under the RG flow they change sign and become ferromagnetic, which promotes the triplet instability. This may be consistent with the experimental observation of a nearby AFM instability in the presence of pressure [17,34–36]. We also note that although J_X, which remains positive under the RG flow, is the smallest term, it is crucial for triplet SC since if it is set to zero we obtain a singlet instability.

V. ORIGIN OF THE CHIRAL SC STATE AND THE ROLE OF SOC

Having established that the C_4 symmetry emerges at the fixed trajectory of the RG flow along with a triplet superconducting order belonging to the 2D E_u irrep of D_{4h}, there remains the question of the relative phase between the two gap functions Δ_H and Δ_V forming the two components of the irrep, since at the level of the one-loop RG flow (or equivalently the linearized gap equation) any linear combination of the two is equivalent. The degeneracy is lifted by the fourth-order term in the free energy

$$\mathcal{F}^{(4)} = \beta_\phi \Delta_V^2 (\Delta_H^*)^2 + c.c. = 2\beta_\phi |\Delta_V|^2 |\Delta_H|^2 \cos 2\phi. \tag{5.1}$$

If β_ϕ is positive, the free energy is minimized by $\phi = \pm\pi/2$ leading to a TRS-breaking chiral order, whereas if β_ϕ is negative the free energy is minimized by $\phi = 0, \pi$, leading to a TRS-preserving phase (see, e.g., Refs. [39,40]; additional terms may instead favor a nematic combination but we assume that is not the case as this is not seen in experiment).

The Feynman diagrams that contribute to this term must contain the two vertices Δ_{BF} and two vertices $\Delta_{LR}^\dagger$ (or vice versa) connected by fermion propagators. This is not possible unless the propagator can change a fermion from a horizontal chain to one on the vertical chain. One possible way this can happen is through the interchain interactions, but one can check that for a triplet order parameter the resulting corrections vanish due to out of plane mirror symmetries. The only other possible way is through SOC: Observe that the symmetry-allowed SOC in Eq. (2.2) couples precisely uranium and tellurium electrons living on horizontal and vertical chains, respectively. The corresponding Green's function is, to leading order in SOC,

$$\begin{aligned} G(i\omega, \mathbf{p}) &= (i\omega - \mathcal{H}_1(\mathbf{p}))^{-1} \\ &= \begin{pmatrix} \frac{1}{i\omega - \varepsilon_U(\mathbf{p})} & \frac{\alpha}{(i\omega - \varepsilon_U(\mathbf{p}))(i\omega - \varepsilon_{Te}(\mathbf{p}))} \\ \frac{\alpha}{(i\omega - \varepsilon_U(\mathbf{p}))(i\omega - \varepsilon_{Te}(\mathbf{p}))} & \frac{1}{i\omega - \varepsilon_{Te}(\mathbf{p})} \end{pmatrix}. \end{aligned} \tag{5.2}$$

Projecting the Green's function onto the $A, A' = L, R, B, F$ patches, we find that the off-diagonal terms are thus given by [41]

$$G_{AA'}(i\omega, \mathbf{p}) = G_{A'A}(i\omega, \mathbf{p}) = \frac{\alpha}{(i\omega - \varepsilon_A(\mathbf{p}))(i\omega - \varepsilon_{A'}(\mathbf{p}))}. \tag{5.3}$$

The resulting fourth-order diagram shown in Fig. 7 corresponds to a free-energy term proportional to

$$\begin{aligned} \beta_\phi &= 8T \sum_{n,\mathbf{p}} G_{BL}^2(i\omega, \mathbf{p}) G_{FR}^2(-i\omega, -\mathbf{p}) \\ &= \sum_{n,\mathbf{p}} \frac{8T\alpha^4}{\big(\omega^2 + \varepsilon_B^2(\mathbf{p})\big)^2 \big(\omega^2 + \varepsilon_L^2(\mathbf{p})\big)^2} \\ &\approx \frac{\alpha^4 \pi^2}{240 T^5} \frac{1}{|v_{F,U}||v_{F,Te}|}, \end{aligned} \tag{5.4}$$

where we took $\varepsilon_B(\mathbf{p}) = -\varepsilon_F(-\mathbf{p}) \approx v_{F,Te} p_y$ and $\varepsilon_R(\mathbf{p}) = -\varepsilon_L(-\mathbf{p}) \approx v_{F,U} p_x$; the momentum integral is done before the Matsubara sum. The factor of eight accounts for the spin

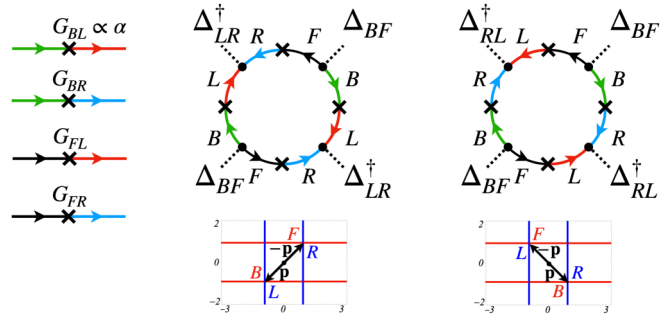

FIG. 7. The fourth-order diagrams that lift the degeneracy of the E_u irrep gap functions (two more diagrams are obtained by exchanging B and F). Note that the diagrams are only allowed when SOC is present, allowing V-chain electrons to change into H-chain electrons and vice versa, giving rise to the off-diagonal Green's functions. For fermions close to the Fermi surface, the conversion can only happen around the four corners where the Fermi surfaces (without SOC) intersect. The kinematics are constrained such that if a B electron in the diagram is converted into an L electron, the electron with opposite momentum is converted from an F electron into an R electron, as indicated in the subplots below.

summation and the fact that there are four contributing diagrams allowed by kinematics. Note that the SOC contributes significantly only around the four points where the quasi-1D Fermi surfaces intersect. The main point, however, is that β_ϕ is positive, so that a chiral TRS-breaking order parameter is favored.

Note that the calculation of the fourth-order term above does not depend at all on the form of the interactions and so applies quite generally regardless of the specific pairing mechanism. In particular, our result is not incompatible with the previously proposed phenomenological explanation of the chirality of the order parameter via coupling to ferromagnetic fluctuations proposed in Refs. [9,14].

VI. DISCUSSION

In this work we have shown that the observed chiral triplet superconductivity in UTe_2 can be explained by a combination of an accidental C_4 symmetry (composed with a PHS) at the level of the noninteracting Hamiltonian together with a resulting *emergent* C_4 symmetry of the interactions. Under the RG flow, a triplet SC order belonging to a 2D E_u irrep is established, and the chiral combination is selected when SOC is included. When the C_4 symmetry is broken, the two components of the E_u irrep descend to a $B_{2u} + iB_{3u}$ chiral combination of irreps of D_{2h}, in agreement with experimental data [9,14].

The quasi-1D nature of the model plays a key role, allowing for a possibility that sans coupling between U and Te chains the system would be in a Luttinger liquid regime, with only marginal interactions in the RG flow. The interchain interactions then tilt the system toward the superconducting instability with an emergent C_4 symmetry. One possible direction for a future study is to attempt a bosonized version of the calculation, since each 1D chain can then in principle be studied exactly [21–23,25,26,42–44]. Additionally, antiferromagnetism has been observed in samples under pressure [17,34–36], which may also be studied using the RG equations presented here and which may compete or be intertwined with the triplet superconducting state. In particular, the 1D chains may enter the Luther-Emery liquid phase in the limit of zero interchain interactions [45], resulting in an AFM or SDW instability. Umklapp processes that we ignored here may also play a significant role.

Within our model we generally neglected the f electrons, which likely play a role in mediating the superconductivity via ferromagnetic fluctuations $\mathbf{M} \sim f^\dagger_\alpha \sigma^z_{\alpha\beta} f_\beta$ or via a recently proposed Hund's-Kondo mechanism [37]. Our model is not incompatible with these scenarios as we do not postulate the origin of the bare couplings, though the RG equations do shed light on what type of microscopic interactions are compatible with the chiral triplet state. It may, therefore, be fruitful to study a more detailed microscopic model of the interactions within the RG framework presented here.

ACKNOWLEDGMENTS

We thank P. Volkov, R. M. Fernandes, and L. Classen for useful discussions and A. Kamenev for referring us to the literature. The authors are especially grateful to A. Chubukov for reading the paper and providing extremely useful feedback. D.S. was supported by startup funds at Emory University. D.V.C. was supported by the Anatoly Larkin and Doctoral Dissertation Fellowships of the University of Minnesota. D.V.C. also acknowledges the hospitality of KITP at Santa Barbara, where this project was initiated. The part of the research done at KITP was supported in part by the National Science Foundation under Grant No. NSF PHY-1748958.

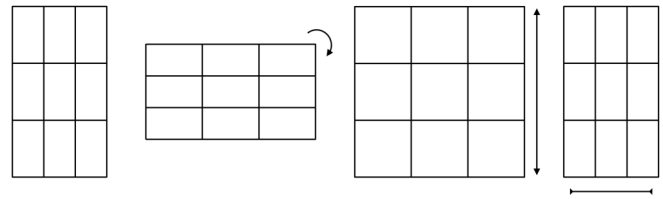

FIG. 8. An extra symmetry of an orthorhombic system of wires: After a C_4 rotation, rescaling along b and a brings the system of wires into the original system of wires. Alternatively, the image represents the BZ in momentum space and the Fermi surfaces. As long as the Fermi momenta of U and Te wires are in the same ratio as a and b, the Fermi surfaces are mapped back to themselves under the same combination of symmetries.

APPENDIX A: SOURCES OF C_4 SYMMETRY BREAKING IN THE FREE HAMILTONIAN

There are several possible sources of C_4 symmetry breaking that we have neglected for simplicity, but two of those can be accommodated within our model by combining C_4 with further symmetries. First of all, the a and b lattice parameters for UTe_2 differ by a significant amount, around 2/3 [18]. Though this does explicitly break C_4 symmetry, for a system of crossed wires C_4 combined with a rescaling along a and b directions remains a symmetry, as shown in Fig. 8 (note that this is not the case for a general orthorhombic system and is a special property of the crossed-wires system; the rescaling can also be thought of as sliding the wires). As long as the Fermi momenta of the U and Te wires have the same ratio as a and b, they also respect this symmetry (see Fig. 8). The ratio of the Fermi momenta does appear to be close to a/b in ARPES data in Ref. [18], and as long as it is not too large there remains an effective C_4-like symmetry.

The second source of C_4 symmetry breaking that can also be accommodated in our model is the difference of densities of states of the U and Te chains. As mentioned in the main text, the difference can be absorbed into the definitions of the coupling constants and vertices, which can be rescaled as $\tilde{g}_V = \nu_V g_V$, $\tilde{g}_H = \nu_H g_H$, $\tilde{g}_X = \sqrt{\nu_V \nu_H} g_X$, $\tilde{\Delta}^{(\mu)}_H = \sqrt{\nu_H}\Delta^{(\mu)}_H$, and $\tilde{\Delta}^{(\mu)}_H = \sqrt{\nu_V}\Delta^{(\mu)}_V$. We note incidentally that the difference in the domains of p_x and p_y discussed above similarly appears in the RG equations as numerical factors that can be absorbed into the density of states. In either case, there is, therefore, still an emergent C_4-like symmetry in the RG equations, but in addition to the C_4 symmetry it includes a rescaling of the d and c operators by $d \to \sqrt{\nu_U/\nu_{Te}}d$ and $c \to \sqrt{\nu_{Te}/\nu_U}c$. Importantly, this is an exact symmetry of the RG equations and our results remain valid modulo the rescaling.

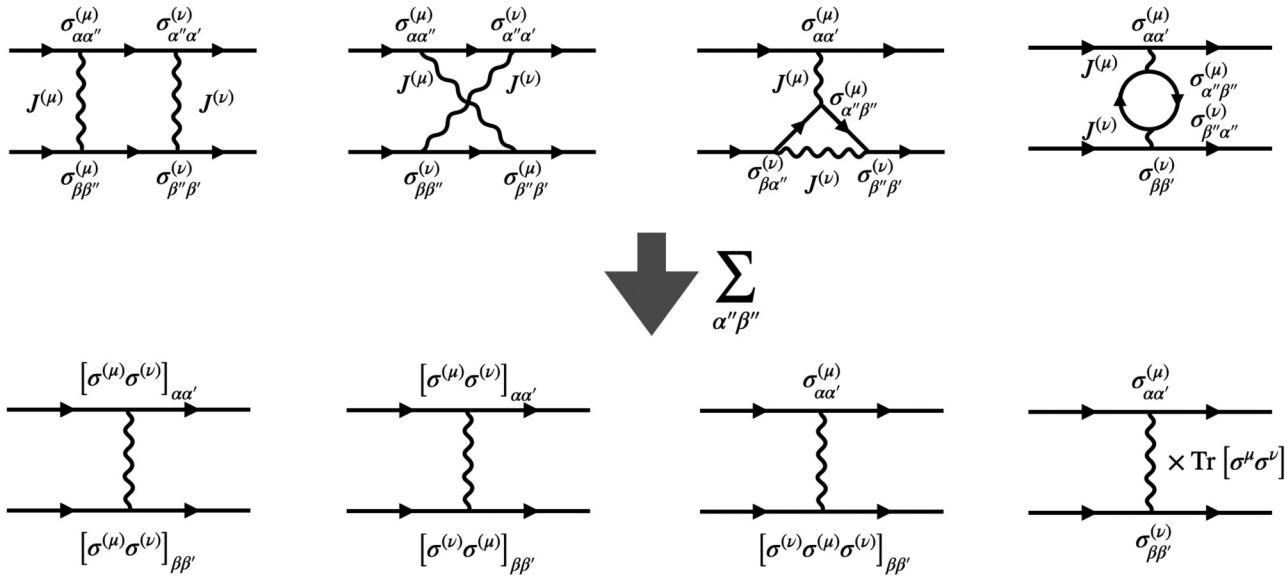

FIG. 9. Spin sums involved in the one-loop diagrams for the RG flow of the coupling constants. Diagrams above contribute to the flow of the diagrams directly below. α' and β' are internal spin indices to be summed over.

APPENDIX B: DETAILS OF THE RG CALCULATION

In this Appendix we show the details of the RG calculation. The one-loop diagrams relevant for the RG flows are shown in Figs. 3 and 4. We need to consider the relevant spin summations, illustrated in Fig. 9. Here we use $\sigma^0 = \delta$ and $J^{(0)} = u$, with $\mu, \nu = 0, x, y, z$. For the ladder diagrams we get

$$J^{(\mu)}J^{(\nu)}[\sigma^{(\mu)}\sigma^{(\nu)}]_{\alpha\alpha'}[\sigma^{(\mu)}\sigma^{(\nu)}]_{\beta\beta'} \tag{B1}$$

For the crossed ladder diagram we get

$$J^{(\mu)}J^{(\nu)}[\sigma^{(\mu)}\sigma^{(\nu)}]_{\alpha\alpha'}[\sigma^{(\nu)}\sigma^{(\mu)}]_{\beta\beta'}. \tag{B2}$$

For the bubble diagram we get

$$J^{(\mu)}J^{(\nu)}\mathrm{Tr}[\sigma^{(\mu)}\sigma^{(\nu)}]\sigma^{(\mu)}_{\alpha\alpha'}\sigma^{(\nu)}_{\beta\beta'} \tag{B3}$$

(this accounts for the usual factor of two, and note that $\mathrm{Tr}[\sigma^{(\mu)}\sigma^{(\nu)}] = 2\delta_{\mu\nu}$). Finally, for the "penguin" diagram we have

$$J^{(\mu)}J^{(\nu)}[\sigma^{(\mu)}\sigma^{(\nu)}\sigma^{(\mu)}]_{\alpha\alpha'}\sigma^{(\nu)}_{\beta\beta'} \tag{B4}$$

with the ν vertex being on the bottom (similarly for the upside down "penguin" diagram). For completeness, Fig. 10 shows the spin sums for the one-loop vertex correction.

Using these, we find the following RG flow equations for the coupling constants within the H chain (see Figs. 3 and 4):

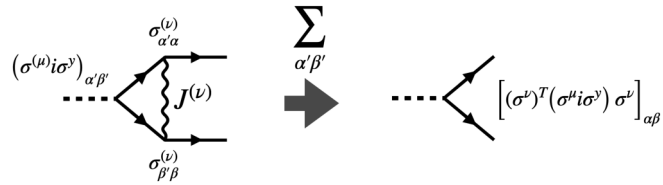

FIG. 10. Spin sums involved in the one-loop diagrams for the RG flow of the particle-particle vertices. The diagram on the left contributes to the flow of the diagram on the right. α' and β' are internal spin indices to be summed over

$$\begin{aligned}
\dot{u}_{1H} &= -u_{2H}^2 + u_{3H}^2 - |\mathbf{J}_{2H}|^2 + |\mathbf{J}_{3H}|^2 - |u_{1X}|^2 - |u_{2X}|^2 - |\mathbf{J}_{1X}|^2 - |\mathbf{J}_{2X}|^2 \\
\dot{u}_{2H} &= -2u_{2H}^2 - 2\mathbf{J}_{1H}\cdot\mathbf{J}_{2H} + 2u_{3H}\sum_j J_{3H}^{(j)} + 2u_{2H}\sum_j J_{1H}^{(j)} - 2\mathrm{Re}[u_{1X}^* u_{2X} + \mathbf{J}_{1X}^*\cdot\mathbf{J}_{2X}] \\
\dot{u}_{3H} &= 4u_{1H}u_{3H} - 2u_{2H}u_{3H} + 2\mathbf{J}_{1H}\cdot\mathbf{J}_{3H} + 2u_{3H}\sum_j J_{1H}^{(j)} + 2u_{2H}\sum_j J_{3H}^{(j)} \\
\dot{J}_{1H}^{(x)} &= 2\left(u_{3H}J_{3H}^{(x)} - u_{2H}J_{2H}^{(x)} + 2J_{1H}^{(y)}J_{1H}^{(z)} + J_{2H}^{(y)}J_{2H}^{(z)} + J_{3H}^{(y)}J_{3H}^{(z)}\right) - 2\mathrm{Re}\left[u_{1X}^*J_{1X}^{(x)} + u_{2X}^*J_{2X}^{(x)} - J_{1X}^{(y)*}J_{1X}^{(z)} - J_{2X}^{(y)*}J_{2X}^{(z)}\right] \\
\dot{J}_{2H}^{(x)} &= 2\left(-u_{2H}J_{1H}^{(x)} - J_{2H}^{(x)2} + J_{2H}^{(y)}J_{1H}^{(z)} + J_{1H}^{(y)}J_{2H}^{(z)}\right) + 2J_{3H}^{(x)}\left(u_{3H} - J_{3H}^{(y)} - J_{3H}^{(z)}\right) + 2J_{2H}^{(x)}\left(J_{1H}^{(x)} - J_{1H}^{(y)} - J_{1H}^{(z)}\right) \\
&\quad - 2\mathrm{Re}\left[u_{1X}^*J_{2X}^{(x)} + u_{2X}^*J_{1X}^{(x)} - J_{1X}^{(y)*}J_{2X}^{(z)} - J_{2X}^{(y)*}J_{1X}^{(z)}\right] \\
\dot{J}_{3H}^{(x)} &= 2\left(2u_{1H}J_{3H}^{(x)} + u_{3H}J_{1H}^{(x)} + J_{1H}^{(y)}J_{3H}^{(z)} + J_{3H}^{(y)}J_{1H}^{(z)} - J_{2H}^{(x)}J_{3H}^{(x)}\right) + 2J_{2H}^{(x)}\left(u_{3H} - J_{3H}^{(y)} - J_{3H}^{(z)}\right) + 2J_{3H}^{(x)}\left(J_{1H}^{(x)} - J_{1H}^{(y)} - J_{1H}^{(z)}\right)
\end{aligned} \tag{B5}$$

The flow equations for $J^{(y)}$ and $J^{(z)}$ are obtained by cyclic permutation from the $J^{(x)}$ equations. The coupling constants within the V chain have the same flow equations with H replaced by V. Observe that even if at the bare level $u = 0$, they are generated

by the J's and so have to be included in the analysis even if we are mostly interested in the spin fluctuations. Observe also that the flows for the umklapp couplings are not affected by the interchain interactions. The interchain coupling constants flow as follows:

$$\begin{aligned}
\dot{u}_{1X} &= -u_{1v}u_{1X} - u_{2V}u_{2X} - u^*_{1X}u_{1H} - u^*_{2X}u_{2H} - \mathbf{J}_{1V}\cdot\mathbf{J}_{1X} - \mathbf{J}_{2V}\cdot\mathbf{J}_{2X} - \mathbf{J}^*_{1X}\cdot\mathbf{J}_{1H} - \mathbf{J}^*_{2X}\cdot\mathbf{J}_{2H}\\
\dot{u}_{2X} &= -u_{1V}u_{2X} - u_{2V}u_{1X} - u^*_{2X}u_{1H} - u^*_{1X}u_{2H} - \mathbf{J}_{1V}\cdot\mathbf{J}_{2X} - \mathbf{J}_{2V}\cdot\mathbf{J}_{1X} - \mathbf{J}^*_{2X}\cdot\mathbf{J}_{1H} - \mathbf{J}^*_{1X}\cdot\mathbf{J}_{2H}\\
\dot{J}^{(x)}_{1X} &= -u_{1V}J^{(x)}_{1X} - u_{1X}J^{(x)}_{1V} - u_{2V}J^{(x)}_{2X} - u_{2X}J^{(x)}_{2V} - u^*_{1X}J^{(x)}_{1H} - u_{1H}J^{(x)*}_{1X} - u^*_{2X}J^{(x)}_{2H} - u_{2H}J^{(x)*}_{2X}\\
&\quad + J^{(y)}_{1V}J^{(z)}_{1X} + J^{(y)}_{2V}J^{(z)}_{2X} + J^{(y)*}_{1X}J^{(z)}_{1H} + J^{(y)*}_{2X}J^{(z)}_{2H} + J^{(z)}_{1V}J^{(y)}_{1X} + J^{(z)}_{2V}J^{(y)}_{2X} + J^{(z)*}_{1X}J^{(y)}_{1H} + J^{(z)*}_{2X}J^{(y)}_{2H}\\
\dot{J}^{(x)}_{2X} &= -u_{1V}J^{(x)}_{2X} - u_{2X}J^{(x)}_{1V} - u_{2V}J^{(x)}_{1X} - u_{1X}J^{(x)}_{2V} - u^*_{2X}J^{(x)}_{1H} - u_{1H}J^{(x)*}_{2X} - u^*_{1X}J^{(x)}_{2H} - u_{2H}J^{(x)*}_{1X}\\
&\quad + J^{(y)}_{1V}J^{(z)}_{2X} + J^{(y)}_{2V}J^{(z)}_{1X} + J^{(y)*}_{2X}J^{(z)}_{1H} + J^{(y)*}_{1X}J^{(z)}_{2H} + J^{(z)}_{1V}J^{(y)}_{2X} + J^{(z)}_{2V}J^{(y)}_{1X} + J^{(z)*}_{2X}J^{(y)}_{1H} + J^{(z)*}_{1X}J^{(y)}_{2H}.
\end{aligned} \tag{B6}$$

Notice that the equations are clearly symmetric under the exchange of H and V, implying that there may be fixed trajectories for which g_H and g_V are equal. Assuming isotropic spin fluctuations then leads to Eq. (4.4).

[1] S. Ran, C. Eckberg, Q.-P. Ding, Y. Furukawa, T. Metz, S. R. Saha, I.-L. Liu, M. Zic, H. Kim, J. Paglione, and N. P. Butch, Nearly ferromagnetic spin-triplet superconductivity, Science **365**, 684 (2019).

[2] L. Jiao, S. Howard, S. Ran, Z. Wang, J. O. Rodriguez, M. Sigrist, Z. Wang, N. P. Butch, and V. Madhavan, Chiral superconductivity in heavy-fermion metal UTe_2, Nature (London) **579**, 523 (2020).

[3] T. Metz, S. Bae, S. Ran, I. Lin Liu, Y. S. Eo, W. T. Fuhrman, D. F. Agterberg, S. M. Anlage, N. P. Butch, and J. Paglione, Point-node gap structure of the spin-triplet superconductor UTe_2, Phys. Rev. B **100**, 220504(R) (2019).

[4] D. Aoki, J.-P. Brison, J. Flouquet, K. Ishida, G. Knebel, Y. Tokunaga, and Y. Yanase, Unconventional Superconductivity in UTe_2, J. Phys. conden. Matter **34**, 243002 (2022).

[5] S. Ran, I.-L. Liu, Yun Suk Eo, D. J. Campbell, P. M. Neves, W. T. Fuhrman, S. R. Saha, C. Eckberg, H. Kim, D. Graf, F. Balakirev, J. Singleton, J. Paglione, and N. P. Butch, Extreme magnetic field-boosted superconductivity, Nat. Phys. **15**, 1250 (2019).

[6] A. G. Lebed, Restoration of superconductivity in high magnetic fields in UTe_2, Mod. Phys. Lett. B **34**, 2030007 (2020).

[7] V. P. Mineev, Reentrant Superconductivity in UTe_2, JETP Lett. **111**, 715 (2020).

[8] M. J. Park, Y. B. Kim, and SungBin Lee, Geometric Superconductivity in 3D Hofstadter Butterfly, arXiv:2007.16205 (2020).

[9] Di S. Wei, D. Saykin, O. Y. Miller, S. Ran, S. R. Saha, D. F. Agterberg, J. Schmalian, N. P. Butch, J. Paglione, and A. Kapitulnik, Interplay between magnetism and superconductivity in ute_2, Phys. Rev. B **105**, 024521 (2022).

[10] M. S. Scheurer, D. F. Agterberg, and J. Schmalian, Selection rules for Cooper pairing in two-dimensional interfaces and sheets, npj Quantum Mater. **2**, 1 (2017).

[11] A. H. Nevidomskyy, Stability of a Nonunitary Triplet Pairing on the Border of Magnetism in UTe_2, arXiv:2001.02699 (2020).

[12] K. Ishihara, M. Roppongi, M. Kobayashi, Y. Mizukami, H. Sakai, Y. Haga, K. Hashimoto, and T. Shibauchi, Chiral superconductivity in UTe_2 probed by anisotropic low-energy excitations, arXiv:2105.13721 [cond-mat] (2021).

[13] T. Shishidou, H. G. Suh, P. M. R. Brydon, M. Weinert, and D. F. Agterberg, Topological band and superconductivity in UTe_2, Phys. Rev. B **103**, 104504 (2021).

[14] I. M. Hayes, Di S. Wei, T. Metz, J. Zhang, Yun Suk Eo, S. Ran, S. R. Saha, J. Collini, N. P. Butch, D. F. Agterberg, A. Kapitulnik, and J. Paglione, Multicomponent superconducting order parameter in UTe_2, Science **373**, 797 (2021).

[15] Y. Xu, Y. Sheng, and Yi-feng Yang, Quasi-Two-Dimensional Fermi Surfaces and Unitary Spin-Triplet Pairing in the Heavy Fermion Superconductor UTe_2, Phys. Rev. Lett. **123**, 217002 (2019).

[16] M. B. Walker and K. V. Samokhin, Model for Superconductivity in Ferromagnetic $ZrZn_2$, Phys. Rev. Lett. **88**, 207001 (2002).

[17] J. Ishizuka and Y. Yanase, Periodic Anderson model for magnetism and superconductivity in UTe_2, Phys. Rev. B **103**, 094504 (2021).

[18] L. Miao, S. Liu, Y. Xu, E. C. Kotta, C.-J. Kang, S. Ran, J. Paglione, G. Kotliar, N. P. Butch, J. D. Denlinger, and L. A. Wray, Low Energy Band Structure and Symmetries of UTe_2 from Angle-Resolved Photoemission Spectroscopy, Phys. Rev. Lett. **124**, 076401 (2020).

[19] D. Aoki, H. Sakai, P. Opletal, Y. Tokiwa, J. Ishizuka, Y. Yanase, H. Harima, Ai Nakamura, D. Li, Y. Homma, Y. Shimizu, G. Knebel, J. Flouquet, and Y. Haga, First observation of de haas-van alphen effect and fermi surfaces in unconventional superconductor UTe_2, arXiv:2206.01363 (2022).

[20] T. Tummuru, O. Can, and M. Franz, Chiral p-wave superconductivity in a twisted array of proximitized quantum wires, Phys. Rev. B **103**, L100501 (2021).

[21] R. Mukhopadhyay, C. L. Kane, and T. C. Lubensky, Crossed sliding Luttinger liquid phase, Phys. Rev. B **63**, 081103(R) (2001).

[22] R. Mukhopadhyay, C. L. Kane, and T. C. Lubensky, Sliding Luttinger liquid phases, Phys. Rev. B **64**, 045120 (2001).

[23] D. G. Shelton, A. A. Nersesyan, and A. M. Tsvelik, Antiferromagnetic spin ladders: Crossover between spin s=1/2 and s=1 chains, Phys. Rev. B **53**, 8521 (1996).

[24] T. Giamarchi and A. M. Tsvelik, Coupled ladders in a magnetic field, Phys. Rev. B **59**, 11398 (1999).

[25] H.-H. Lin, L. Balents, and M. P. A. Fisher, N-chain Hubbard model in weak coupling, Phys. Rev. B **56**, 6569 (1997).

[26] H.-H. Lin, L. Balents, and M. P. A. Fisher, Exact SO(8) symmetry in the weakly-interacting two-leg ladder, Phys. Rev. B **58**, 1794 (1998).

[27] S. Raghu, Suk Bum Chung, and S. Lederer, Theory of textquotesinglehiddentextquotesingle quasi-1D superconductivity in Sr_2RuO_4, J. Phys.: Conf. Ser. **449**, 012031 (2013).

[28] P. Coleman, A. M. Tsvelik, N. Andrei, and H. Y. Kee, Cooperative two-channel kondo effect, J. Phys.: Condens. Matter **10**, L239 (1998).

[29] A. M. Tsvelick and P. B. Wiegmann, Solution of then-channel kondo problem (scaling and integrability), Z. Phys. B **54**, 201 (1984).

[30] N. Andrei and C. Destri, Solution of the Multichannel Kondo Problem, Phys. Rev. Lett. **52**, 364 (1984).

[31] P. Coleman and A. J. Schofield, Simple Description of the Anisotropic Two-Channel Kondo Problem, Phys. Rev. Lett. **75**, 2184 (1995).

[32] M. Fabrizio, A. O. Gogolin, and Ph. Nozières, Crossover from Non-Fermi-Liquid to Fermi-Liquid behavior in the Two Channel Kondo Model with Channel Anisotropy, Phys. Rev. Lett. **74**, 4503 (1995).

[33] M. S. Dresselhaus, G. Dresselhaus, and A. Jorio, *Group Theory: Application to the Physics of Condensed Matter* (Springer-Verlag, Berlin, Heidelberg, 2008).

[34] C. Duan, K. Sasmal, M. B. Maple, A. Podlesnyak, J.-X. Zhu, Q. Si, and P. Dai, Incommensurate Spin Fluctuations in the Spin-Triplet Superconductor Candidate UTe_2, Phys. Rev. Lett. **125**, 237003 (2020).

[35] W. Knafo, G. Knebel, P. Steffens, K. Kaneko, A. Rosuel, J.-P. Brison, J. Flouquet, D. Aoki, G. Lapertot, and S. Raymond, Low-dimensional antiferromagnetic fluctuations in the heavy-fermion paramagnetic ladder UTe_2, Phys. Rev. B **104**, L100409 (2021).

[36] S. M. Thomas, F. B. Santos, M. H. Christensen, T. Asaba, F. Ronning, J. D. Thompson, E. D. Bauer, R. M. Fernandes, G. Fabbris, and P. F. S. Rosa, Evidence for a pressure-induced antiferromagnetic quantum critical point in intermediate-valence UTe_2, Sci. Adv. **6**, eabc8709 (2020).

[37] T. Hazra and P. Coleman, Triplet pairing mechanisms from hund's-kondo models: applications to UTe_2 and $CeRh_2As_2$, arXiv:2205.13529 (2022).

[38] We again assume equal DOS's on H and V chains, but this difference can again be taken into account by rescaling the vertices as $\tilde{\Delta}_H^{(\mu)} = \sqrt{\nu_H}\Delta_H^{(\mu)}$ and $\tilde{\Delta}_H^{(\mu)} = \sqrt{\nu_V}\Delta_V^{(\mu)}$. See Appendix A.

[39] R. M. Fernandes, P. P. Orth, and J. Schmalian, Intertwined Vestigial Order in Quantum Materials: Nematicity and Beyond, Annu. Rev. Condens. Matter Phys. **10**, 133 (2019).

[40] S. Maiti and A. V. Chubukov, $s + is$ state with broken time-reversal symmetry in Fe-based superconductors, Phys. Rev. B **87**, 144511 (2013).

[41] There are additional diagrams due to SOC and interactions that do not affect the analysis. For example, the lowest-order correction to free energy in α is $\sim\alpha^2\Delta^2$. The four possible contributions are:

$$F^{(2)}(\alpha) \sim \alpha^2(\Delta_{LR}\Delta_{FB}^* + \Delta_{RL}\Delta_{FB}^*) + \text{c.c.}$$

However, this sum vanishes for spin-triplet pairing because of the symmetry relations of gap functions IV.13.

[42] A. M. Tsvelick and P. B. Wiegmann, Exact results in the theory of magnetic alloys, Adv. Phys. **32**, 453 (1983).

[43] N. Andrei, K. Furuya, and J. H. Lowenstein, Solution of the Kondo problem, Rev. Mod. Phys. **55**, 331 (1983).

[44] A. O. Gogolin, A. A. Nersesyan, and A. M. Tsvelik, *Bosonization and Strongly Correlated Systems* (Cambridge University Press, Cambridge, 2004).

[45] A. Luther and V. J. Emery, Backward Scattering in the One-Dimensional Electron Gas, Phys. Rev. Lett. **33**, 589 (1974).